# Analysis of thermal response and electrical characterisation of triple-junction solar cells based on variable solar spectral irradiance and air mass

# Accepted Manuscript

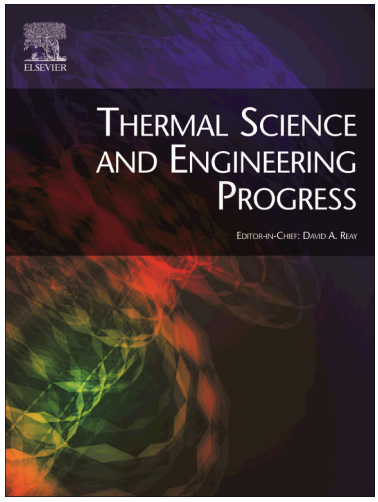


Analysis of thermal response and electrical characterisation of triple-junction solar cells based on variable solar spectral irradiance and air mass

Ali O. M. Maka, Tadhg S. O'Donovan

PII: S2451-9049(18)30015-5
DOI: https://doi.org/10.1016/j.tsep.2019.02.005
Reference: TSEP 309

To appear in: *Thermal Science and Engineering Progress*

Received Date: 9 January 2018
Revised Date: 26 December 2018
Accepted Date: 19 February 2019

Please cite this article as: A. O. M. Maka, T.S. O'Donovan, Analysis of thermal response and electrical characterisation of triple-junction solar cells based on variable solar spectral irradiance and air mass, *Thermal Science and Engineering Progress* (2019), doi: https://doi.org/10.1016/j.tsep.2019.02.005

# Analysis of thermal response and electrical characterisation of triple-junction solar cells based on variable solar spectral irradiance and air mass

**Ali O. M. Maka*, Tadhg S. O'Donovan**

Institute of Mechanical, Process and Energy Engineering, School of Engineering and Physical Sciences
Heriot-Watt University, Edinburgh, EH14 4AS, United Kingdom
*Corresponding author email: aom2@hw.ac.uk.

## Abstract

This paper presents the effects of Air Mass (*AM*) on solar cell performance. This atmospheric parameter has a strong influence on the behaviour of high concentrating photovoltaic solar cells. As air mass increases, the Direct Normal Irradiance (*DNI*) decreases and resulting cell temperature ($T_c$) decrease. The objective of this work is to assess the effects of air mass (*AM* =1-10D) on triple-Junction solar cells. A thermal model using a convergent iterative technique has been developed; the predicted convergent cell temperature is ≤ 80°C for the range of parameters tested. The rate of heat loss by convective heat transfer from the cell is also considered for air mass values *AM* =1.5, 4 and 8D. A Finite Element Method (FEM) model is developed in COMSOL Multiphysics in order to predict the temperature distribution on PV cells and the thermal behaviour of the receiver assembly. The proportion of the absorbed radiation not converted to electricity is converted to heat; also, heat from potential current mismatch resulting in an increase in cell temperature is taken into account. As the air mass increases, results show that the spectral attenuation has a significant effect on the thermal and electrical conversion efficiency of triple-junction solar cells. In addition, spectral change is one of the causes of the current mismatch in triple-junction cells. Thus, cell parameters such as short current density ($J_{sc}$), efficiency and output power are affected.

**Keywords:** thermal response, air mass, triple-junction cells, convergent cell temperature, concentrating Photovoltaic.

## 1. Introduction

The third generation of photovoltaic solar cells are made from layers of III-V semiconductor materials stacked on top of each other. Each layer has a different bandgap, and therefore the cell can yield high efficiencies by exploiting a wide range of the solar spectrum [1, 2]. III-V multi-junction solar cells are still very expensive for terrestrial applications, although, the use of inexpensive optical concentrators can reduce the cells' area and decrease the overall system cost [3, 4]. The performance of HCPV (High Concentration photovoltaics) strongly relies on the internal behaviour of the solar cells, hence, the performance parameter of *DNI*, *AM* etc. have significant influence [5]. The Air mass (*AM*) varies throughout the day, resulting in significant changes in the spectral distribution and *DNI* on the Earth's surface [6].

The solar spectrum is influenced by atmospheric parameters such as clouds, aerosol and perceptible water vapour, but the main factor that affects the solar spectrum is air mass [7]. Subsequently, this affects the multi-junction solar cell's performance. Increases in air mass weakens the solar irradiance over the entire short-wave

spectrum; the relative weakening is greater in the spectral region of the top junction subcell [8]. The increase of *AM* leads to significant deformation of the solar spectrum comprising global sunshine [9].

For multi-junction cells, there are two major issues, which comes from spectral mismatch between the conversion response and the solar spectrum. Firstly, the mismatch leads to the heat generation when the energy photon absorption higher than the energy bandgap. Second issue occurs from that lower photons energy those lower than energy band gaps, thus the photons are not absorbed to be converted to electricity [10].

Senthilarasu et al. [11] investigated the influence of *AM* variation from 1-10D on the spectral irradiance. Because of the growth in attenuation of solar irradiance and distribution of photons density, different *AM* values tend to lower the performance of the solar cell. Reduced performance is visible for Perovskite solar cells for increasing *AM* because of the weakening of solar irradiance and distribution of photo density. Overall, higher *AM* can lead to a photon distribution shift into short wavelength light regions, which affects the solar cell's conversion efficiency. Broderick et al. [12] performed a comparative study of tandem junction and spectral splitting for a parallel junction. The SPCTRAL2 model was used in the calculation for one year, under a concentration of 500x. The comparative modelling study concluded that the daily and yearly mean efficiency of the parallel junction is higher than that of the tandem cell.

Cell temperature under high concentration can be estimated using $V_{oc}$ and $J_{sc}$ parameter measurements. It has been established that the performance of multi-junction solar cells is heavily dependent on cell temperature [13]. Hence, it can be utilised for outdoor investigations of a CPV employed under natural sunlight to calculate the average cell temperature [14]. Theristis et al. [15] investigated the sensitivity of concentrating triple-junction solar cells to the solar spectral. In their numerical study, the effects of solar spectrum distribution change, due to atmospheric parameters such as aerosol optical depth, perceptible water and air mass were reported. In addition, case studies performed on four locations in the US, Typical Meteorological Year (TMY3) were used to calibrate the thermal and electrical performance of a III-V cell at 500x. Further to this study, the current research will predict the thermal response of a cell for a range of convective transfer coefficients to maintain a cell temperature of $\leq 80\ ^{o}C$, and a range of air mass values *AM* of =1.5, 4 and 8D.

Cell and module temperatures in HCPV are affected by atmospheric parameters such as wind speed, air temperature and *DNI* [16, 17]. Consequently, many scholars followed different methods to estimate the cell temperature. Theristis and O'Donovan [18, 19] have reported that in concentrating photovoltaic systems, the cooling requirements should be designed for air mass values less than *AM*1.5D. The prediction of the heat transfer coefficient required from the rear of the cell to the ambient environment temperature is required to design an assembly that maintains safe and efficient operation.

For high concentrating photovoltaics, thermal management is essential to minimise electric conversion efficiency losses, to prevent thermal damage, and to prolong the cell's lifetime. The heat generated in the solar cells can be removed by either active or passive cooling. Furthermore, optimisation of the assembly configuration can be application specific, where both heat and electrical energy are required. There are several techniques available to passively cool solar cells, such as heat sinks and heat spreaders etc. [20]. High concentrating photovoltaic system required appropriate cooling to maintain an operating temperatures at or

below 80 °C [21, 22]. Long-term exposure of solar cells to high optical concentration level without sufficient cooling can lead to higher temperatures which will in turn decreases the lifetime of the cells [23].

In this work, the thermal performance response is predicted for cell temperatures at a concentration ratio of 1000x, based on a thermal model at different atmospheric parameters of *AM* (1.5, 4, 8D). Espinet-González et al [23] have reported that it is necessary to reduce the cell temperature below safe operating limits for cell integrity. However, long-term degradation or reliability concerns should consider an operating temperature of 80°C instead of 100°C. To do so, in the study we used a spectrum irradiance model SMARTS2 to simulate different *AM* (1, 1.5, 4, 6, 8 and 10D). The spectrum irradiance is integrated across the entire range of wavelengths for different AM values. Furthermore, a performance assessment of their effects on the solar cell is considered by plotting *J-V* and *PV* characteristic curves for electrical parameters such as cell power density and efficiency. The current study differs from available studies by reporting on the thermal performance response of the cell subject for a range of *AM* values (1.5, 4 and 8D) at different environment temperature (25 to 45 $^{o}$C) for a range of convective heat transfer coefficients. The numerical thermal-electrical model has been developed using a convergent iterative technique to determine the steady-state temperature of the cell. A Finite Element Method (FEM), using COMSOL Multiphysics is employed to predict the cell temperature and the temperature distribution of the receiver assembly.

## Nomenclature

| | |
|---|---|
| $A_c$ | Area of the cell ($m^2$) |
| $A_s$ | Convective area ( $m^2$ ) |
| CR | Concentration Ratio (x) |
| *DNI* | Direct Normal Irradiance ($W/m^2$) |
| $E_g$ | Energy band gap (eV) |
| G | Solar direct irradiance ($W/m^2/nm$) |
| $h_{conv}$ | Convection heat transfer coefficient ($W/m^2K$) |
| $J_{sc}$ | Short circuit current density ($A/cm^2$) |
| $J_o$ | Dark current density (A) |
| $k_b$ | Boltzmann constant (eV/K) |
| *m* | Mass of the cell (g) |
| *n* | Diode ideality factor (-) |
| $P_{out}$ | Amount of delivered power (W) |
| $P_{in}$ | Incident Power (W) |
| $Q_{cm}$ | heat generated due to current mismatch (W) |
| *q* | Electron charge ( c) |
| $q_{heat}$ | Heat power (W) |
| $Q_{out}$ | Heat dissipated from the cell (W) |
| *Q* | Amount heat in cell after dissipation (W) |
| $R_s$ | Series resistance (Ω ) |
| *SR* | spectrum response (A/W ) |
| $T_{C1}$ | Initial cell temperature ($^oC$) |
| $T_{C2}$ | Final cell temperature ( $^oC$) |
| $T_{amb}$ | Ambient temperature ($^oC$) |
| $T_o$ | Temperature at standard condition ( $^oC$) |
| $T_C$ | Cell temperature ($^oC$ ) |
| $V_{oc}$ | Open circuit voltage (V) |
| $x_c$ | Cell thickness |

**Greek symbols**

| | |
|---|---|
| ρ | Density |
| $\eta_c$ | Cell efficiency |
| λ | wavelength (nm) |
| α | Material constant (eV/K) |
| β | Material constant ( K) |
| $\beta_\eta$ | Efficiency temperature coefficient |
| γ | Materials constant (-) |
| K | Materials constant ($A/cm^2K^4$) |
| ε | surface emissivity |
| σ | Stefan–Boltzmann constant |
| $\eta_{opt}$ | Optical efficiency |
| k | Thermal conductivity K(W/(mK)) |

**Abbreviations**

| | |
|---|---|
| GaInP | Gallium Indium Phosphide |
| GaInAs | Gallium Indium Arsenide |
| Ge | Germanium |
| *AM* | Air Mass |
| FEM | Finite Element Method |
| SMART2 | Simple model of Atmospheric Radiative Transfer version 2 |
| FF | Fill Factor |
| HCPV | High Concentrating Photovoltaic |
| DBC | Direct Bend Cupper |
| $Al_2O_3$ | Aluminium Oxide |
| EQE | External Quantum Efficiency |
| CPV | Concentrating photovoltaic |

## 2. Methodology

The modelling approach is summarised in the flow diagram in Figure-1. Direct spectral irradiance is calculated using version2 SMARTS (Simple Model of Atmospheric Radiative Transfer of Sunshine) model for different *AM* values [24, 25]. The SMARTS2 takes the spectrum of an ASTM 173-G as an input and calculates the solar spectrum distribution for Air Mass values ranging from *AM* =1-10D. By integrating the solar irradiance over the range of wavelengths the magnitude of the *DNI* can be calculates as a function of *AM*, and therefore the zenith angle.

An electrical model of a GaInP/GaInAs/Ge triple-junction solar cell was developed to evaluate the solar cell performance according to the changes in spectral irradiance. The performance of the solar cell was characterised by *J-V* curves. A current mismatch occurred between subcells where there was spectral weakness; the current limitation is variable, based on the values of *AM*.

To predict cell temperature as a function of *AM* values, a thermal model was developed in MATLAB. The heat power is generated from the solar power not converted to electricity and current mismatch due to current limitation. The ambient temperature is considered in the prediction of the cell operating temperature for a range of $h_{conv}$. Additionally, a steady state thermal model was developed using a Finite Element Method (FEM) in COMSOL Multiphysics software, in order to predict cell and receiver assembly temperature distribution.

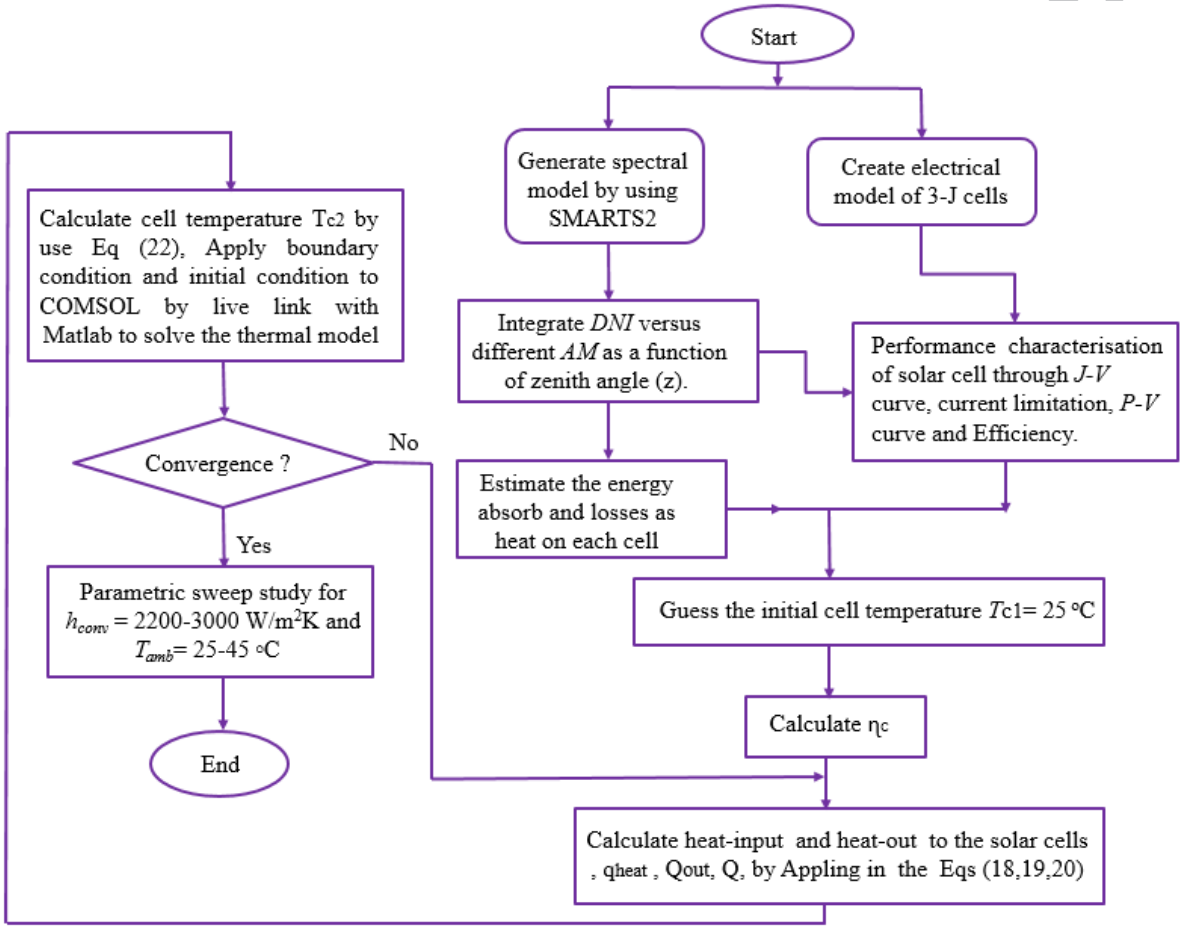


**Fig.1** Flow diagram of process and the steps of the proposed modelling.

## 3. Models description

### 3.1.Spectrum model

The direct spectral irradiance has been generated from the SMARTS2 model. The integration of the spectral irradiance at a specific air mass gives the irradiance intensity as a function of the zenith angle (z). Other parameters were kept constant at the reference conditions of the standard ASTM G173-03 (Gueymard and Myers) [26]. The design of the multi-junction solar cell needs an accurate prediction of solar incident spectral irradiance on the model concentrator. For this application of the module, in a dry climate, the SMARTS2 model is considered a suitable tool to predict the spectral irradiance [24, 27].

### 3.2. Electric model of (GaInP/GaInAs/Ge)

A solar cell is, in principle, a semiconductor material; based on p-n junctions it is designed to generate current from the absorption of light energy photons. A simple electrical model of three monolithically stacked layers or sub-cells was created in MATLAB. The subcells were connected in series, with multiple single-junctions of semiconductor materials III-V, single cells and diodes. Usually, the solar cell performance is characterised by *J-V* curves. The short circuit current density generated in each subcell is determined by the incident light spectrum by considering an incident irradiance with spectrum response for certain wavelengths. Moreover, the integration across the entire range of wavelengths of the subcells areas are considered and given in equation (1) [28].

$$J_{sc(\lambda)} = \int_{\lambda 1}^{\lambda 2} G_{(\lambda)}.SR_{(\lambda)}.\eta_{opt}\,d\lambda \tag{1}$$

Where $G$ is incident spectrum irradiance, $\eta_{opt}$ is the optical efficiency and $SR$ is the spectrum response, which is defined as " amperes generated per watt of incident light for given a wavelength" [29]. It considers wavelength responses ranging from (300nm-1800nm), as expressed by the relationship in Eq. (2):

$$SR_{(\lambda)} = \frac{q.\lambda}{h.c}.EQE_{(\lambda)} \tag{2}$$

Where $q$ is the electron charge, EQE is external quantum efficiency, λ is photon wavelength, $c$ is the speed of light and $h$ is the Planck constant. Reverse saturation current $J_o$ is also affected by the band gap reduction, which results in a decrease in open circuit voltage and the given temperature; the $J_o$ is given by Eq. (3) [15].

$$J_o = K.T_c^{(3+\frac{\gamma}{2})} \exp\frac{-E_g}{n.K_b.T_c} \tag{3}$$

Where $K_b$ is the Boltzmann constant, $n$ is the diode ideality factor; γ and K are materials constant in each layer. The band gap energy of semiconductor materials can be calculated by the Varshni equation (4). The Varshni empirical relation [30] gives the temperature dependence of semiconductor band gaps.

$$E_{g(T),i} = E_{g,i}(0) - \frac{\alpha_i.T_c^{\,2}}{T_c + \beta_{,i}} \tag{4}$$

Where $E_g(0)$ is the band gap at 0 K, the index $i$ represents the sub-cell of each layer, $T_c$ is the cell temperature and α and β are material constants. The total current is determined by subtracting the light-induced current from the diode dark current, given by Eq. (5):

$$J = J_o\left(\exp\frac{q(V + J.R_s)}{n.K_b.T_c} - 1\right) - J_{sc} \tag{5}$$

Where $R_s$ is a series resistance, $V$ is the voltage and $J_{ph}$ is the photocurrent; in an ideal case the photocurrent is equal to the short circuit density $J_{ph} = J_{sc}$. Because of the series connection, the overall current of the three layers is given by the lower current density as expressed in relationship Eq (6):

$$J_{total} = \min(J_1, J_2, J_3) \tag{6}$$

Equation (7) used to calculate the open circuit voltage $V_{oc}$.

$$V_{oc} = \frac{n.K_b.T_c}{q} \ln\left(\frac{J_{sc}}{J_0} + 1\right) \tag{7}$$

Equation (8) is the relationship to determine the voltage produced by each subcell. The total voltage is the sum of three subcells as per Eq. (9):

$$V = \frac{n.K_b.T_c}{q} \ln\left(\frac{J_{sc} - J}{J_0} + 1\right) - J.A_c.R_s \tag{8}$$

$$V_{total} = \sum_{i=1}^{3} V, i \tag{9}$$

The Fill Factor (*FF*), defined as the ratio of the maximum output power $P_{max}$ from the solar cell to the product of its open circuit voltage and short-circuits current is given in Eq. (10):

$$FF = \frac{P_{\max.}}{V_{oc}.J_{sc}} \tag{10}$$

The efficiency represents the percentage ratio between the power output and the power input as expressed by Equation (11), where $\eta_{el}$ is the cell electrical efficiency, $P_{out}$ is the amount of delivered power and $P_{in}$ is the quantity of incident power on the solar cell.

$$\eta_{el} = \frac{p_{out}}{P_{in}} = \frac{J_{sc}.V_{oc}.FF}{\int G.A_c.CR.\eta_{opt}} \tag{11}$$

The concentration ratio achieved by means of the proportional rise of short circuit current intensity, can be expressed in electric terms as follows:

$$J_{sc(X)} = J_{sc,1X}.CR \tag{12}$$

The open circuit voltage increases logarithmically with concentration ratio as given in Equation (13):

$$V_{oc}(x) = V_{oc} + \frac{n.k_b.T_c}{q} \ln(CR) \tag{13}$$

### 3.3. Thermal finite element model

A finite element thermal model using COMSOL Multiphysics, together with an electrical model, iteratively solves partial differential equations [31] to determine the thermal distribution throughout the cell assembly. The receiver assembly consists of the solar cell on Direct Copper Bonded (DCB) substrate. The DCB is made of copper/$Al_2O_3$ ceramic/copper and silver used for electrical connections. Aluminum is selected for its good equilibrium between thermal performance, weight, and cost [5, 32]. Fig. 2 illustrates the main receiver assembly configuration and boundary conditions and Table-1 lists all boundary conditions and assumptions. The heat dissipated by conduction through the receiver of the solid component is given by Fourier's law (14):

$$q_{con} = -k\nabla T \tag{14}$$

Where $k$ is thermal conductivity and $q_{con}$ is conductive heat flux. The amount of heat dissipated by convection is expressed in equation (15) by Newton's law of cooling:-

$$q_{conv} = h_{conv}.A_s.\Delta T \tag{15}$$

The heat loss by radiation cooling, which transfers heat electromagnetically to the environment is given by equation (16):

$$q_{rad} = \varepsilon.\sigma.(T_s^4 - T_{amb}^4) \tag{16}$$

where $q_{rad}$ is radiative heat transfer, $T_s$ is surface temperature, ε is the surface emissivity and σ is the Stefan–Boltzmann constant.

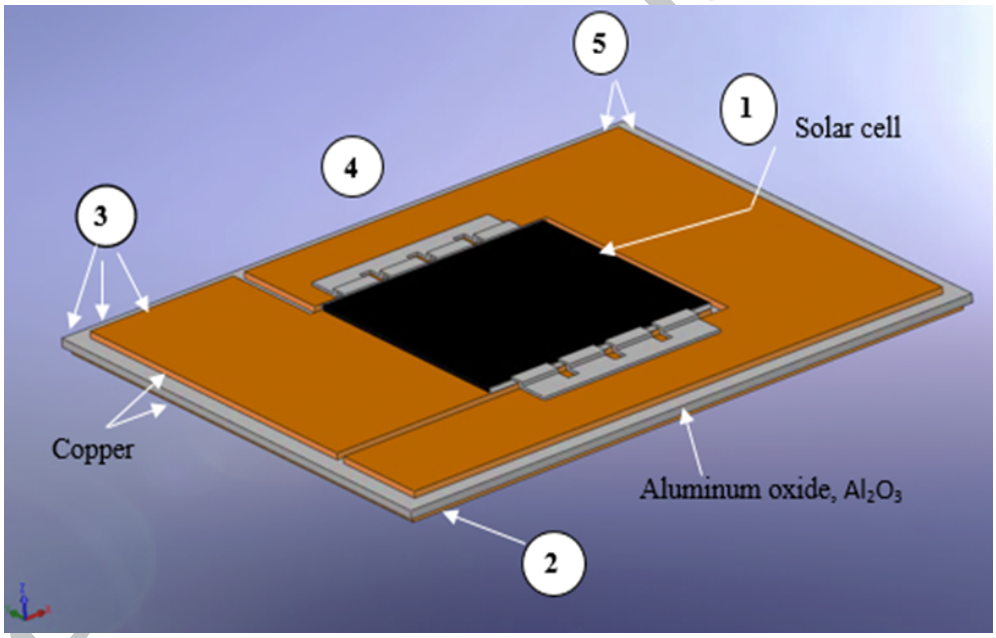


**Fig.2** Receiver assembly component structures and boundary condition.

**Table.1** listed boundary condition.

| No | boundary condition |
|---|---|
| 1 | Triple cells (the heat source). |
| 2 | Rear plate convection heat transfer = 2200 - 3000W/m$^2$K. |
| 3 | Natural convection of all free surface. |
| 4 | Ambient temperature =25-45 $^o$C. |
| 5 | Surface radiation. |

### 3.4. MATLAB Thermal Model

In order to estimate the cell temperature, a numerical model written in MATLAB script is solved iteratively, beginning with the first approximation of the cell temperature $T_{c1}$. The cell operating temperature is expressed by Eq.(17) [33]. It is estimated from electrical parameters, with consideration of the concentration ratio and environment temperature.

$$T_c^* = T_{amb} + \frac{V_{oc}(x) - V_{oc}}{\beta_{Voc}} \tag{17}$$

where $T_c$* is the cell operating temperature, $T_{amb}$ is the environment temperature and $\beta_{Voc}$ is the open circuit temperature coefficient. Equation (18) [34, 35] is used to calculate the cell conversion efficiency $\eta_c$ as a function of temperature, where $\eta_{el}$ is the cell electric efficiency for the concentration ratio, $\beta_\eta$ is an efficiency temperature coefficient, and $T_o$ is reference condition temperature.

$$\eta_c = \eta_{el}\left[1 - \beta_\eta (T_c^* - T_o)\right] \tag{18}$$

The amount of heat power in the solar cell from the radiant heat transfer in the solar spectrum is given by Eq.(19) [36, 37], where $q_{heat}$ is the heat power and CR is a concentration ratio.

$$q_{heat} = DNI_{(AM)}.(1-\eta_c).A_c.CR.\eta_{opt} \tag{19}$$

Heat is dissipated by free or forced convection by applying either a passive or active cooling technique. Newton's law states that the convective loss is proportional to the difference in temperature between the surface and the fluid [38]. Convective heat transfer depends on cell mounting, wind conditions and properties of the surrounding air. The amount of heat removed by convection is given by Eq. (20).

$$Q_{out} = h_{conv}.A_s.\Delta T \tag{20}$$

where $Q_{out}$ is the heat dissipated from the cell by convection, $h_{conv}$ is the convective heat transfer coefficient, $(A_s)$ is the convective surface area and $\Delta T$ is the temperature difference between the rear surface temperature and the ambient temperature. $Q$ is the amount of heat in the cell after the heat dissipation; therefore, the cell operating temperature estimation is determined as expressed in Eq (21):

$$Q = q_{heat} - Q_{out} \tag{21}$$

The steady state cell temperature is obtained by adding the initial cell temperature to the total heat generated and is expressed in Eq. (22), where $T_{c2}$ represents steady state cell temperature, $C_p$ is heat capacity and $m$ is the mass of the cell, as given in relationship (23), where $x_c$ is the thickness of the cell, $A_c$ is the cell area and $\rho$ is a material density of the solar cell.

$$T_{c2} = T_{c1} + \frac{Q}{m.Cp} \tag{22}$$

$$m = x_c.A_c.\rho \tag{23}$$

## 4. Results and discussions

### 4.1. Effects of increases of *AM* in the solar spectrum

Air mass is a measure of how absorption in the atmosphere affects the spectral content and intensity of the solar radiation reaching the Earth's surface. It is described as a ratio between the optical path length, and the optical path length when the sun is at the zenith. Fig. 3 illustrates the variation of air mass, which results in significant changes in the spectral distribution of direct irradiance at the surface of the Earth. When air mass increases (1, 1.5, 4, 6 and 10D), the solar intensity decreases, the wavelength becomes shorter and that yields a shift in the direct spectrum.

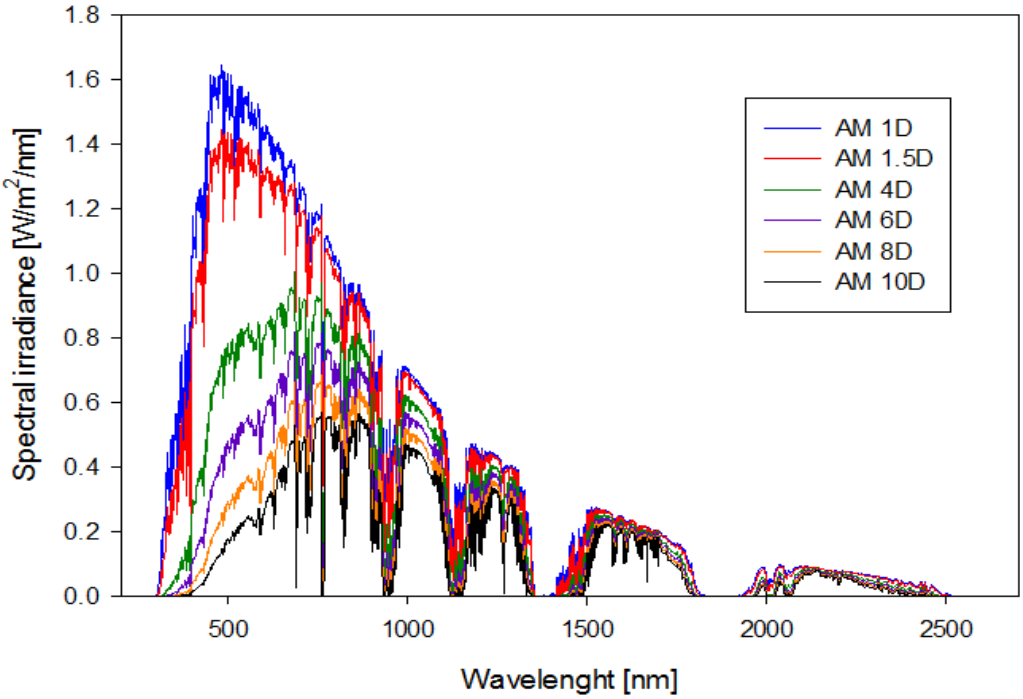


**Fig.3** Direct spectral irradiance generated by SMARTS2 model for different *AM* value.

The performance of the spectral model is dependent on the air mass and the associated parameter with the length of the sunlight path through the Earth's atmosphere. The minimum *AM* value occurs on a clear-sky day, when the Sun is on the noon-time, while the maximum occurs when the Sun is at the sunrise and sunset. The increase towards larger *AM* values is related to the red shift in the solar spectrum. Hence, a *decrease* in *AM* values corresponds to a *rise* in the blue solar spectrum component [6].

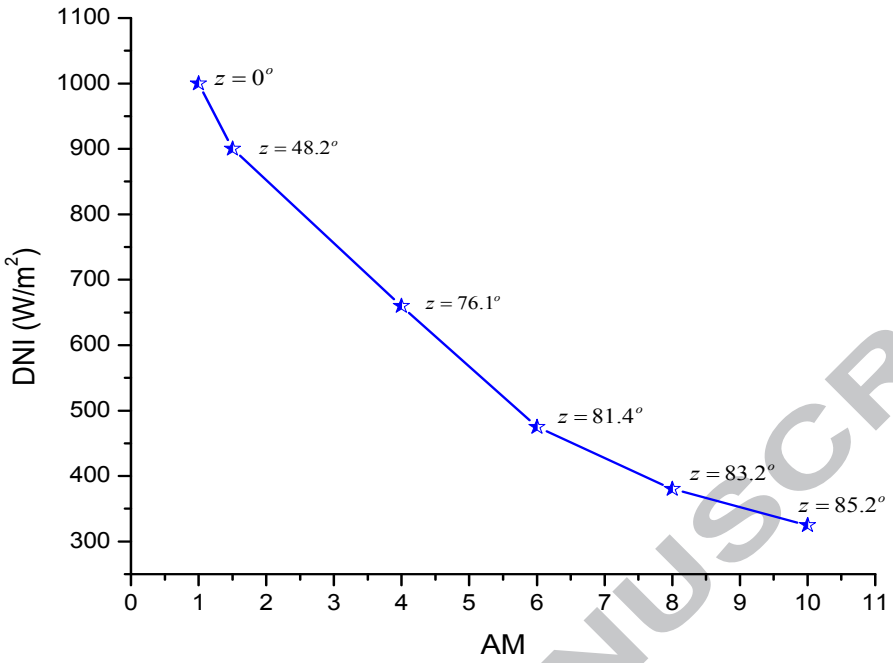


**Fig.4** *DNI* integration versus Air Mass as a function of the zenith angle (z).

Fig. 4 shows the Direct Normal Irradiance at six values of air mass (1, 1.5, 4, 6 and 10D) at different zenith angles, which vary between 0° and 85°. As the zenith angle increases, the integrated *DNI* magnitude decreases. Also, a decrease of the spectral irradiance will lead to attenuation in the wavelengths of incident illumination. The impacts of increasing the sunlight zenith angle is that it vanishes in the short wavelength. This results in an increase in the red shift of the direct solar spectrum. The increase in spectral extinction at lower wavelengths is controlled by scattering from aerosols and molecules [6]. Therefore an increase in the air mass value results in an attenuation of the amount of incident power [39].

### 4.2. Current limitation, *J-V, P-V* and efficiency

The one-diode model is deemed to be an optimum way to practically describe the performance of triple junction solar cells. For triple junction solar cells, the top and bottom cells' series connection is influenced by changes of spectrum which result in a current mismatch and a reduction in overall current density [9]. A subcell has a small energy bandgap, resulting in solar spectrum photon absorption, which produces a small voltage and high current density. However, the *J-V* curve is used to characterise the performance of a cells' parameters. The changes in the solar spectrum from the reference spectrum results in one of the subcells governing and/limiting the overall solar cell current [39]. The ideal performance will occur when their current density is balanced as shown in Fig.5.

The optimum performance under spectrum (G-173-03) *AM* 1.5D, usually occurs when the top and middle cells have been designed to generate equal current density, or "current match". The change in the solar spectrum results in one of the two cells becoming current limited [40]. Also, at a high operating temperature as the cell temperature increases, the middle subcell generates less current; consequently, current limitation shifts to the middle subcell [41]. Therefore, at lower values of *AM* the top and middle junctions generate the same currents

and at higher *AM* values, the top junction will govern overall current; this is because of a decrease in the spectral factor of multi-junction cells [29].

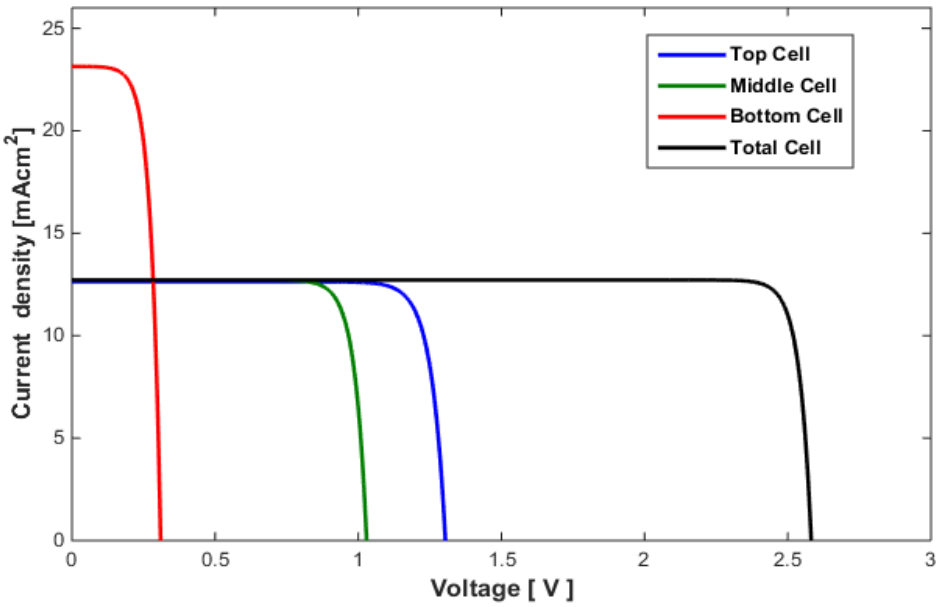


**Fig. 5** *J-V* curve of a combination the top, middle, bottom subcell of tandem 3-Junction, the total current of solar cell limited by top and middle cell at CR= 1x, $T$ = 25 $^{o}$C and *AM* =1.5D.

As shown in Fig. 6, the triple-junction solar cell assembly is very sensitive to changes in the solar spectrum; this is because of the monolithic stack of the subcells. There is a significant reduction in the maximum power density as *AM* increases from 1-10D, as depicted in Fig.7. Higher *AM* leads to lower maximum power; conversely, higher power is achieved at lower *AM* values. Air mass has the most significant influence on the performance of single/multi-junction solar cells. This atmospheric parameter should therefore always be borne in mind while designing or modelling solar cells because of the spectral effects of the incident solar irradiance cause a reduction in the electric output of the cell/module and system of the HCPV [42-44].

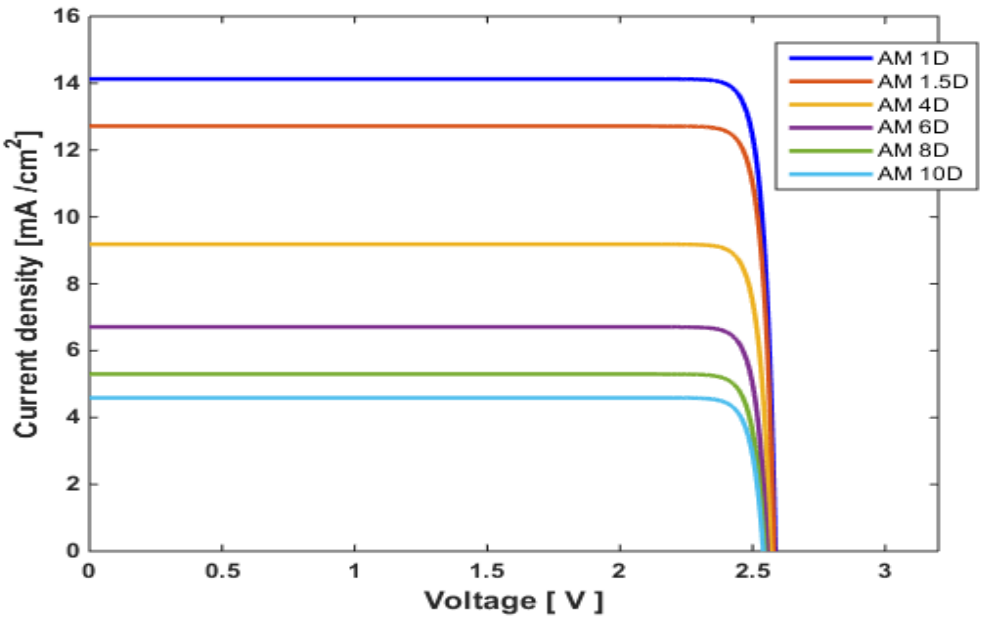


**Fig.6** *J-V* curves of triple-junction cells and effects of variety of air mass.

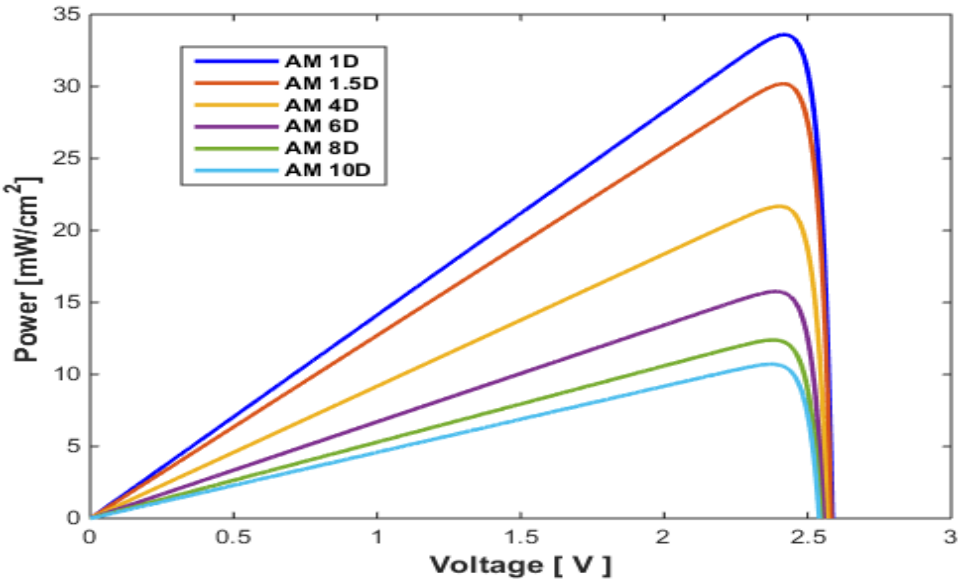


**Fig.** 7 *P-V* curves of triple junction cells and effects of a range of air masses.

Due to the attenuation of the wavelengths in the atmosphere, when the value of air mass increases, the current density reduces and cell efficiency of the multi-junction solar cell decreases. Fig. 8 illustrates how the increases in *AM* has a significant effect on the overall efficiency of a triple-junction solar cell. This is because the energy photons in the solar spectrum decreases. Furthermore, the value of *DNI* decreases as the *AM* values increases. For an increase in air mass value up to *AM* =10D, the cell efficiency drops to 25%. In contrast, with the optimum value of air mass *AM* =1.5D, CR=1x, the cell efficiency stands at 32%.

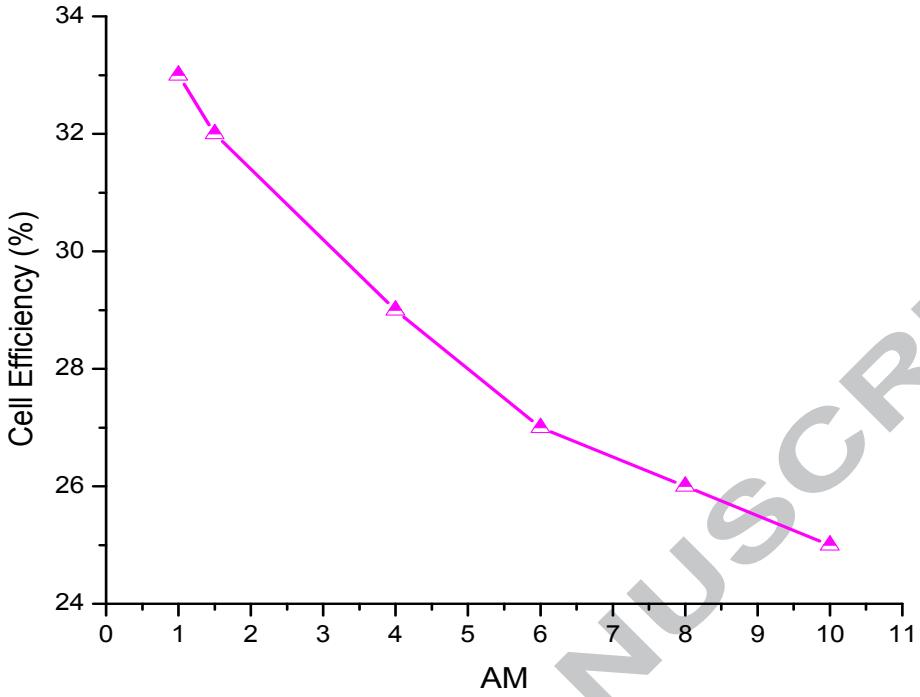


**Fig.8** Influence of air mass variation on cell efficiency.

### 4.3. Estimation of energy conversion yield

Standard test conditions for a solar cell are *DNI* = 1000 W/m$^2$ at *AM*1.5D, $T_{amb}$=25 $^o$C, while the standard operating conditions are *DNI* = 900 W/m$^2$, ambient temperature $T_{amb}$ = 20 $^o$C at *AM*1.5D [27, 45]. In this study the External Quantum Efficiency (EQE) measurement data is taken from Kinsey and Edmondson CM1 [40]. The EQE corresponds to the absorbing spectrum response.

The top cell (GaInP) absorbs the part of the solar spectrum, which contains the ultraviolet and visible wavelength. It responds between approximately 300-700nm wavelength with $E_g$ = 1.8(eV). The middle (GaInAs) layer absorbs the near infrared spectrum. It responds between approximately 700-900nm wavelength with $E_g$ = 1.4(eV). The bottom (Ge) subcell absorbs lower photon energies in the infrared spectrum between 900 and 1800nm with $E_g$ = 0.7(eV). The photon absorption is quantified by the energy gap of the semiconductor material alloy and its absorption coefficient [46]. In order to predict the energy available to be absorbed by each subcell, the EQE as a function of irradiance utilised is expressed in Eq. (24). The amount of energy lost from an incident spectrum occurs in absorption and some by incident spectrum reflection.

$$G_{in(\lambda),i} = \int_{280}^{4000} G_{(\lambda)} \cdot \int_{300}^{1800} EQE_{(\lambda),i} . d\lambda \tag{24}$$

$$DNI_{abso(AM)} = \int G_{abso(\lambda),i} - \left(Th_{losses,i} + Q_{cm,i}\right) \tag{25}$$

where $G_{abso}$ is the amount of an incident spectrum absorbed and converted to electricity by each subcell, $Th_{losses}$ are the thermal losses. The portion of the energy absorbed depending on the air mass, $DNI_{abso}$ ($AM$) by the three junctions of the solar cells and is converted to electricity as expressed by Eq. (25).

The radiation not converted to electricity is lost as heat and results in an increase of solar cell temperature. The thermal losses in the solar cell occur where the absorption of energy is greater or less than the bandgaps [10, 47]. In a triple junction cell, due to a series connection, the total current of the three sub-cells are limited by the minimum. The amount of energy not converted to electrical energy is wasted as heat, as given in equation (26) [10, 19], based on current limitation and spectrum variation effects at different $AM$.

$$Q_{cm} \le \sum_{i=1}^{3} \left[ J_{sc,i} - J_{total} \right] V_{oc,i} \tag{26}$$

where $Q_{cm}$ is heat generated due to current mismatch and $J_{sc}$ is the short current circuit in each layer. The $J_{total}$ is the total current of the three cells, $V_{oc}$ is the open circuit voltage of each layer. The majority of the heat produced due to current limitation comes from the bottom subcell which generates the highest current. The total estimated energy wasted is produced by adding the heat generated because of current mismatch to the energy losses from the incident spectrum.

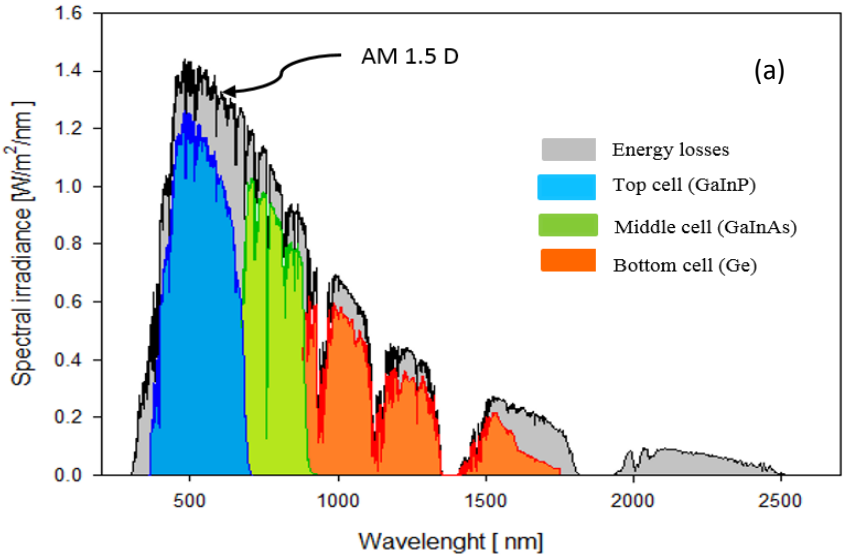


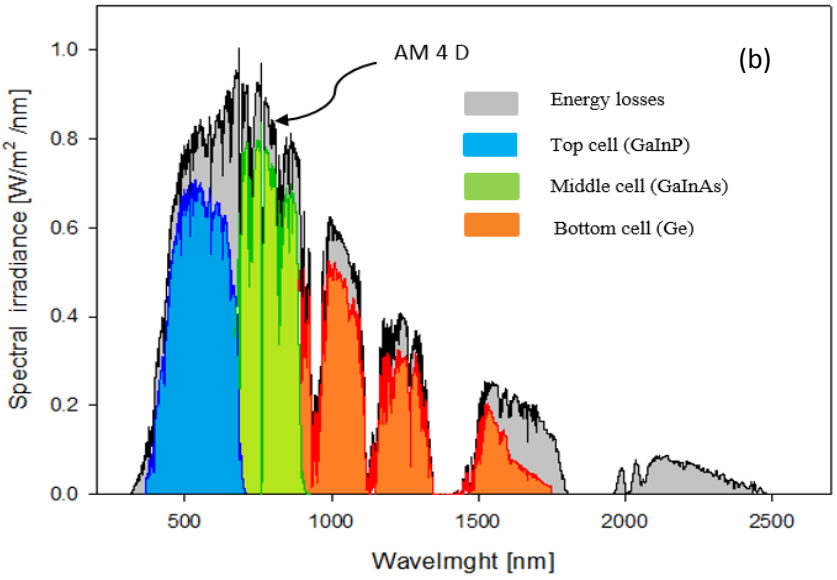


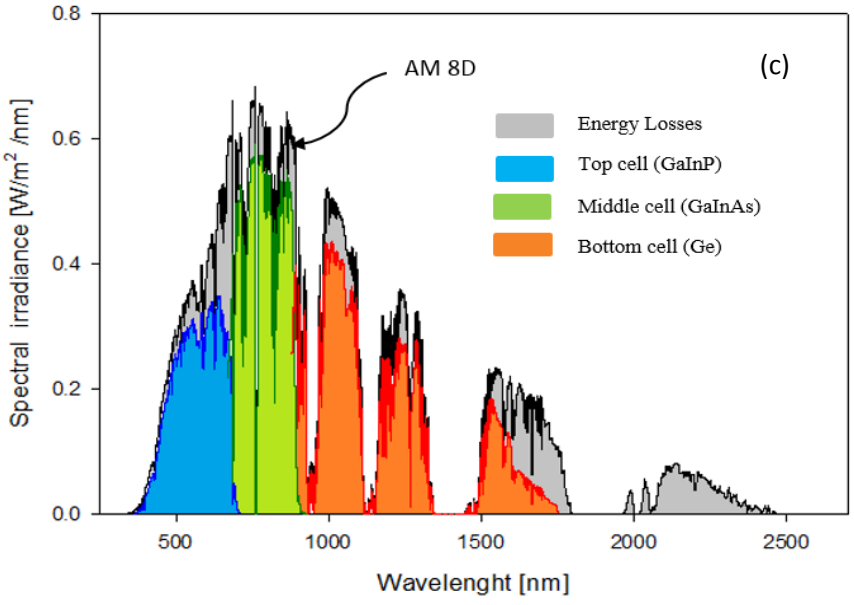

**Fig. 9.** Estimation of portions energy absorbs and approximation of energy losses by each layer of triple-junction cells (a) for *AM* 1.5D, (b) for *AM* 4D and (c) for *AM* 8D.

The available incident power that responds at each range for each subcell (GaInP/GaInAs/Ge) is shown in Fig.9 at different air mass values *AM* (1.5, 4 and 8D). The energy greater than the bandgaps is wasted. Adding different semiconductor materials is one way to utilise such solar spectrum losses and minimise the heat generated. High *AM* values lead to less incident power; as shown in the (lower) figure at *AM* 8D, the Ge layer will produce less power compared with *AM* 1.5D.

4.4 Validation

Model parameter results of the current study were compared to other work; some of the parameters of fill factor FF and efficiency are compatible with the values presented in reference [48]. The results are also shown compatible with parameters of efficiency and $V_{oc}$ open circuits voltage values that presented by Green *et al.*[49]. The efficiency was 32% at 1x; this value in good agreement with an experimental measured value reported in the literature [50]. Table 2 summarised list of performance parameters published in the literature compared with the current study model.

**Table. 2** summarised simulated *J-V* parameters compared to world record values published in the literature for a lattice-matched (LM) MJSC by M. Green et al.[49] and A. Walker [48] triple cell model results, the temperature at 25 °C and concentration of one- sun.

| Parameters | Current study | Model by A. Walker [48] | Error (%) | World Record M. Green et al. [49] | Error (%) |
|---|---|---|---|---|---|
| $J_{sc}$ ($_{m}$Acm$^2$) | 12.6 | 12.3 | 2.3 | 13.2 | 3 |
| $V_{oc}$ (V) | 2.6 | 2.628 | 1 | 2.691 | 2.9 |
| FF(%) | 88 | 87.2 | 0.9 | 86.0 | 2.3 |
| η [%] | 32 | 31.3 | 0.7 | 32.1 | 0.1 |

In the thermal validation aspect, a model of receiver assembly at the condition of *AM* 1.5, CR= 1000x, have similar results presented in the modelling and experimental which is consistent, and in good agreement with the experimental by Muron *et al.*[51]. In addition, there is a good agreement with a modelling prediction which presented by Maka and Donovan [52]. So for the cooling requirement, the value of $h_{conv}$ =2.4 kW/m$^2$K, at $T_{amb}$= 25 $^{o}$C is used.

### 4.5. Analysis of the thermal model

The concentration ratio used in this thermal model is 1000x, where 1x =1000 W/m$^2$. In HCPV, a cooling system is needed to remove heat from the cells, for safety and reliability reasons. It is recommended that the cell operating temperature is maintained at or less than 80 $^o$C. The amount of heat produced must be equal to that removed heat from the cells in order to prevent the temperature from rising, and to allow the system to work under steady-state conditions [5]. The temperature of a solar cell is quantified by incident power and ambient temperature, and influenced by cell efficiency. The amount of heat power generated in the solar cell is given by Eq (19).

As described in Section 2, an iterative solution is required to determine the steady-state condition of the solar cell. An initial cell temperature $T_c$ =25 $^o$C is used and then calculations are based on the input heat generated the cells and convected from the cell surface. The new cell temperature is then calculated using COMSOL's live-link for MATLAB. To solve the model, numerous steps are repeating in order to converge on a solution. The cell temperature stabilises at the point where the generated heat is equivalent to the heat dissipated by the cooling mechanism. The convergence occurs at the steady-state condition, when the iterative ($T_c$) relative error is < 0.1%. The receiver configuration set at the bottom convective area is about 5.13x10$^{-4}$ m$^2$ and the solar cell area is 1cm$^2$. The optimum geometry mesh is a normal size and free triangle type. The completed mesh consists of 92300 number of elements, including domains and boundaries.

The simulation was carried out by using (GMRES) Generalized Minimum Residual, which is an iterative solver to solve general linear systems. It can be observed that while solving a problem with an iterative method, the error estimated in the solution decreases with the increase in the number of iterations [53]. Fig. 10 illustrates the convergence of the solver for *AM* 1.5D, 4D and 8D. For AM1.5D a convective heat transfer coefficient $h_{conv} \geq$ 2.4 kW/m$^2$K is required to maintain cell operating temperature less than 80 $^o$C and converges after approximately 12 iterations. The black trend represents the cell temperature at *AM* 4D. In this case, a convective heat transfer coefficient $\geq$ 2.3kW/m$^2$K is required to maintain the temperature blow the limit; the solution converges after approximately 11 iterations. The orange trend represents a cell temperature at *AM* 8D and a $h_{conv}$ $\geq$ 2.2 kW/m$^2$K is required, and converges after approximately 10 iterations. Table-3 summarised the details of parameters of the efficiency, $h_{conv}$ and $q_{heat}$ versues to the range of *AM* values.

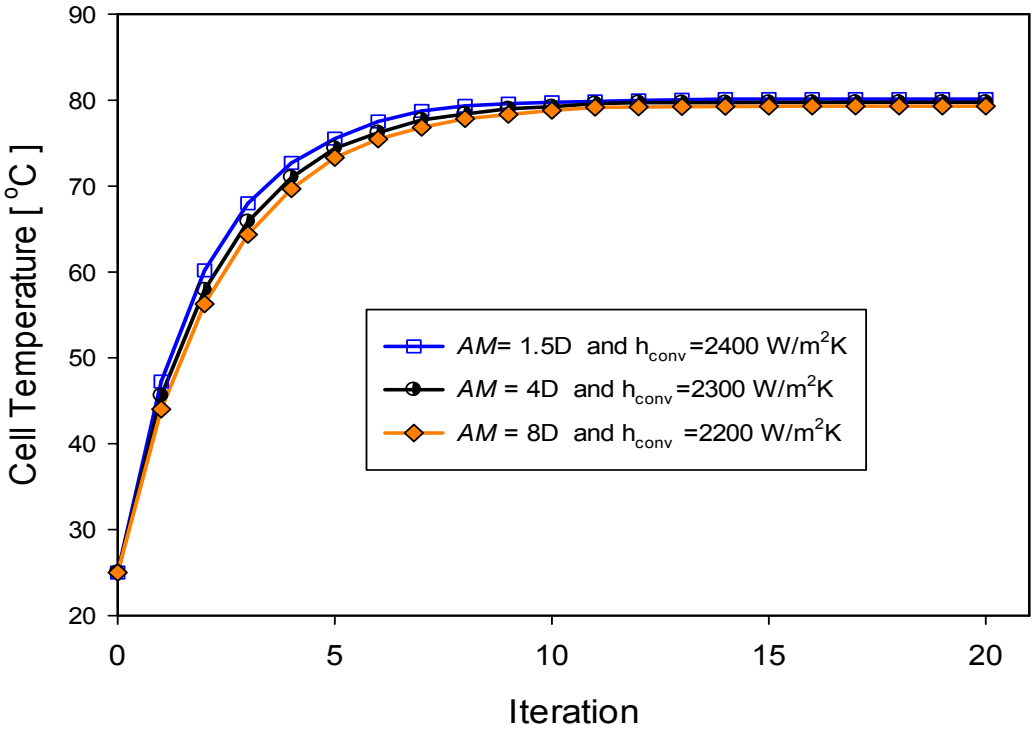


**Fig.10.** Cell convergence temperature versus iterations; this model is of 3-junction cells, at variation of $h_{conv}$ between 2200 to 2400 W/m$^2$K to maintain a cell temperature below 80 °C.

**Table.3** listed different *AM* versus cell temperature converges with different $h_{conv}$ and $T_{amb}$ 25 °C @1000x.

| *AM* | Efficiency (%) | $q_{heat}$ [W] | $h_{conv}$ [ W/m$^2$] |
|---|---|---|---|
| 1.5D | 39 | 50 | 2400 |
| 4D | 37 | 45 | 2300 |
| 8D | 35.5 | 41 | 2200 |

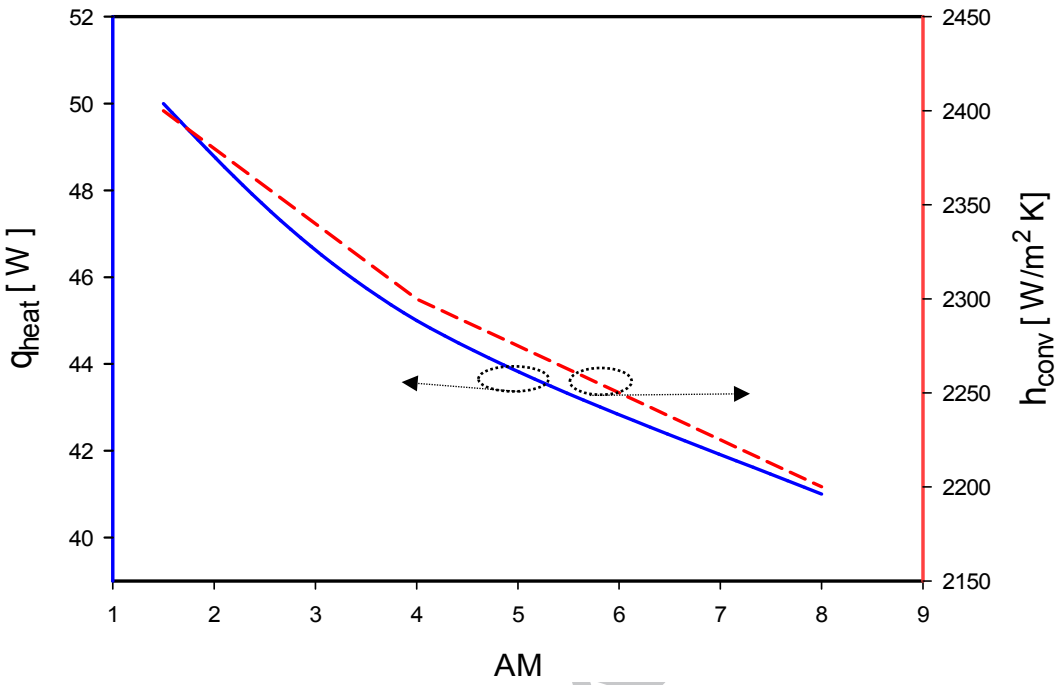


**Fig.11**. *AM* as a function of irradiance versus heat power on the solar cell, also *AM* versus $h_{conv}$ required to maintain a cell temperature below 80 °C.

The heat power as a function of the efficiency of the cell is directly proportional to heat transfer coefficient. As *AM* increases from 1.5 to 8D both $q_{heat}$ and the required $h_{conv}$ decrease significantly as illustrates in Fig.11 . To maintain a cell operating temperature below 80 °C, the value of $h_{conv}$ remarkably decreases as *AM* increases. This is due to the increase of *AM* which results in the cell efficiency dropping, which subsequently leads to decreases in the heat power generated. A multi-junction solar cell can operate above 1000x due to its effectiveness at high temperature [54]. Passive cooling is often applied to concentrating photovoltaic systems ranging from 300-1000x and operating temperatures between 50-80 °C [41, 55].

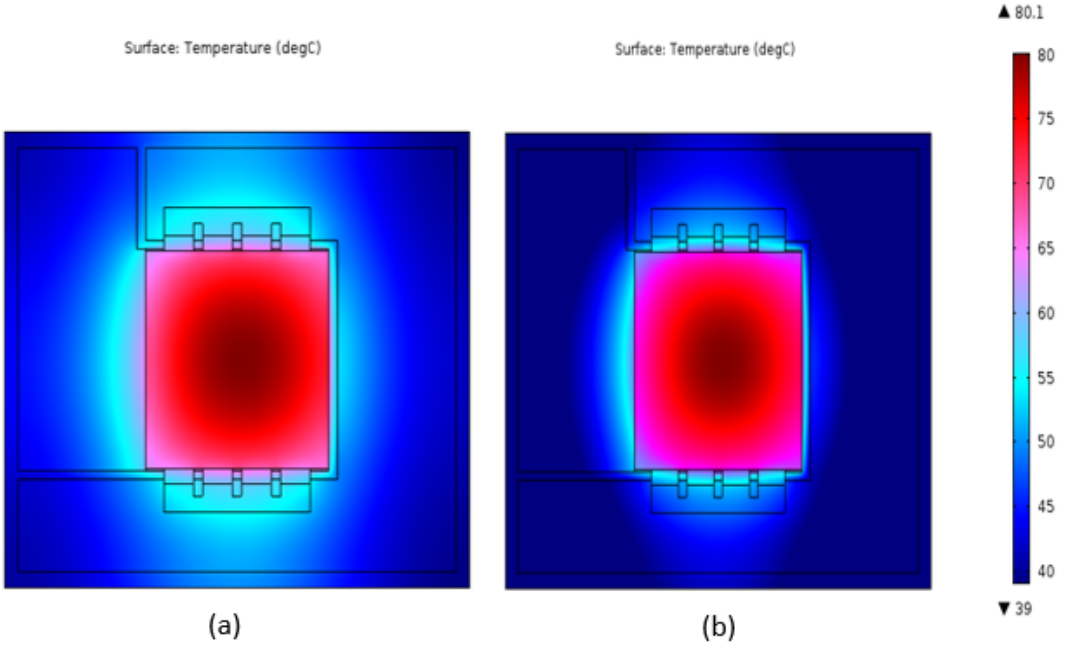


**Fig. 12** 2D plot of temperature distributions on CPV receiver, (a) *AM* 1.5D and at ambient temperature of 25 $^{o}$C, $h_{conv}$ =2400 W/m$^2$K. (b) *AM* 1.5D at ambient temperature of 45 $^{o}$C and $h_{conv}$=3000 W/m$^2$K.

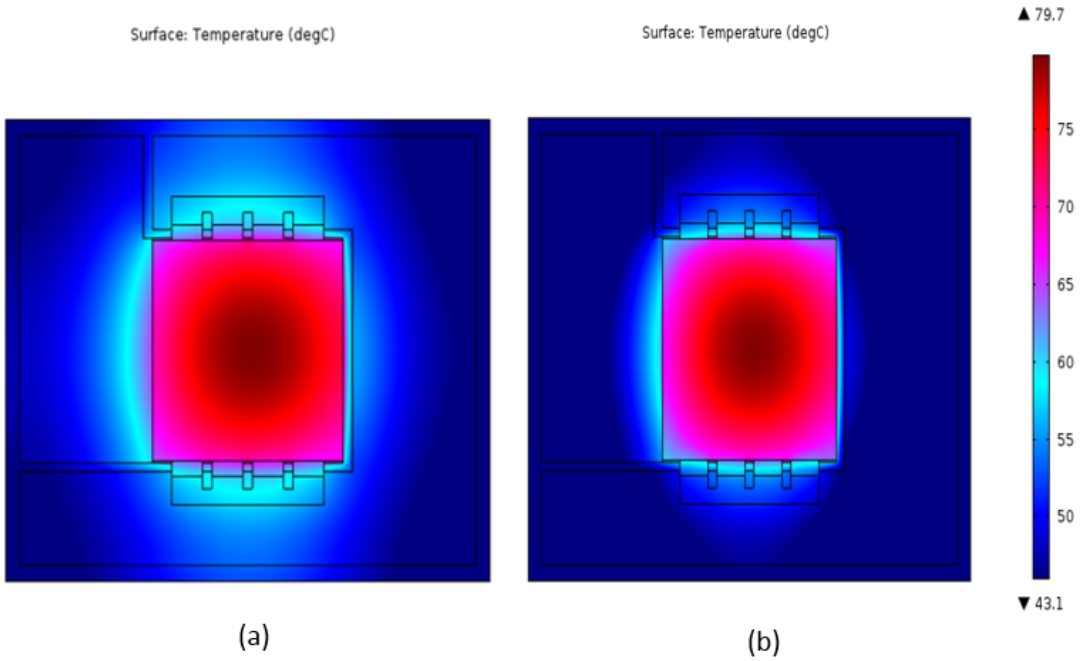


**Fig. 13** 2D plot of temperature distributions on CPV receiver, (a) *AM* 4D, $h_{conv}$= 2300 Wm$^2$K and ambient temperature of 25 $^{o}$C. (b) *AM* 4D and $h_{conv}$ =2800 Wm$^2$K at ambient temperature of 45 $^{o}$C.

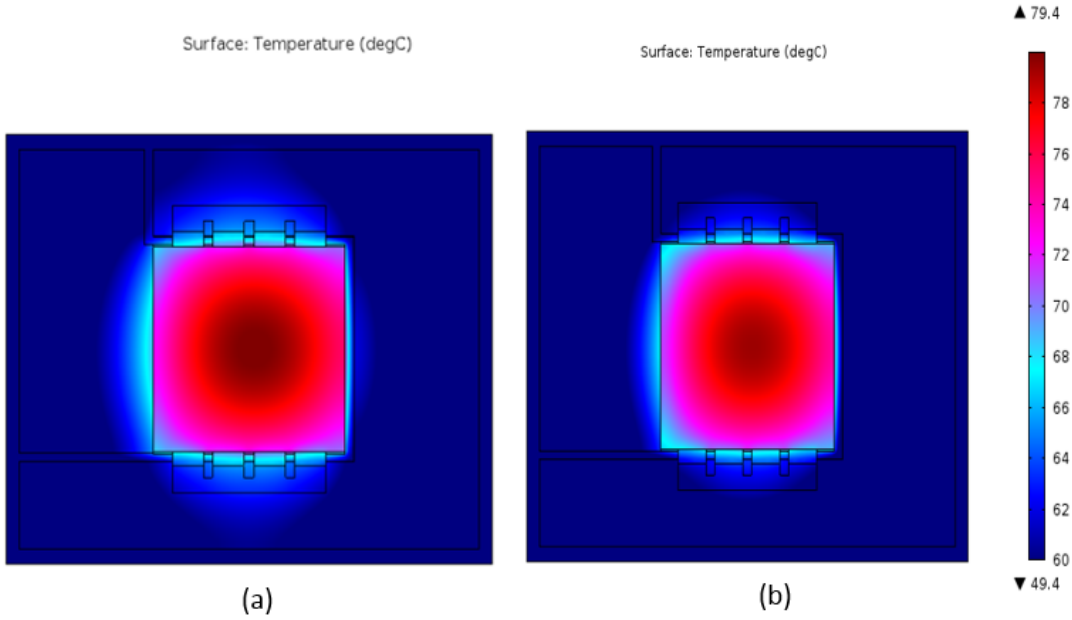


**Fig. 14** 2D plot of temperature distributions on CPV receiver, (a) *AM* 8D and ambient temperature of 25 °C and $h_{conv}$ =2200 W/m²K. (b) *AM* 8D for ambient temperature of 45 °C and $h_{conv}$ =2600 W/m²K.

In order to predict cell temperature or the thermal behaviour as a function of the ambient temperature and *AM, a* parametric sweep study was conducted for $T_{amb}$ =25 to 45 °C and $h_{conv}$ =2200 to 3000 W/m²K. Fig 12-(a) shows the 2D plot of temperature distribution on the receiver of $h_{conv}$ = 2400 W/m²K, an ambient temperature of 25 °C and *AM*1.5D to keep the cell operating temperature below 80 °C. The highest cell temperature occurs at the centre of the cell and the temperature decreases towards the receiver edge. Figure12-(b) is the 2D plot of temperature distribution on the receiver for $h_{conv}$ =3000 W/m²K, and an ambient temperature of 45 °C and *AM* 1.5D.

Fig 13 and 14 illustrate the temperature distribution on the receiver for range of $h_{conv}$ =2200, 2300, 2600, 2800 W/m²K, ambient temperatures of 25 °C, 45 °C and *AM* 4D, 8D. The main significant features in figures (12-14) are summarised, hence as $T_{amb}$ changes from 25-45 °C, the values of $h_{conv}$ rapidly increases in order to keep cell temperature below certain values. In contrast, increases of air mass *AM* =1.5, 4, 8D leads to a reduction in the required values of $h_{conv}$ to maintain a cell temperature below 80 °C.

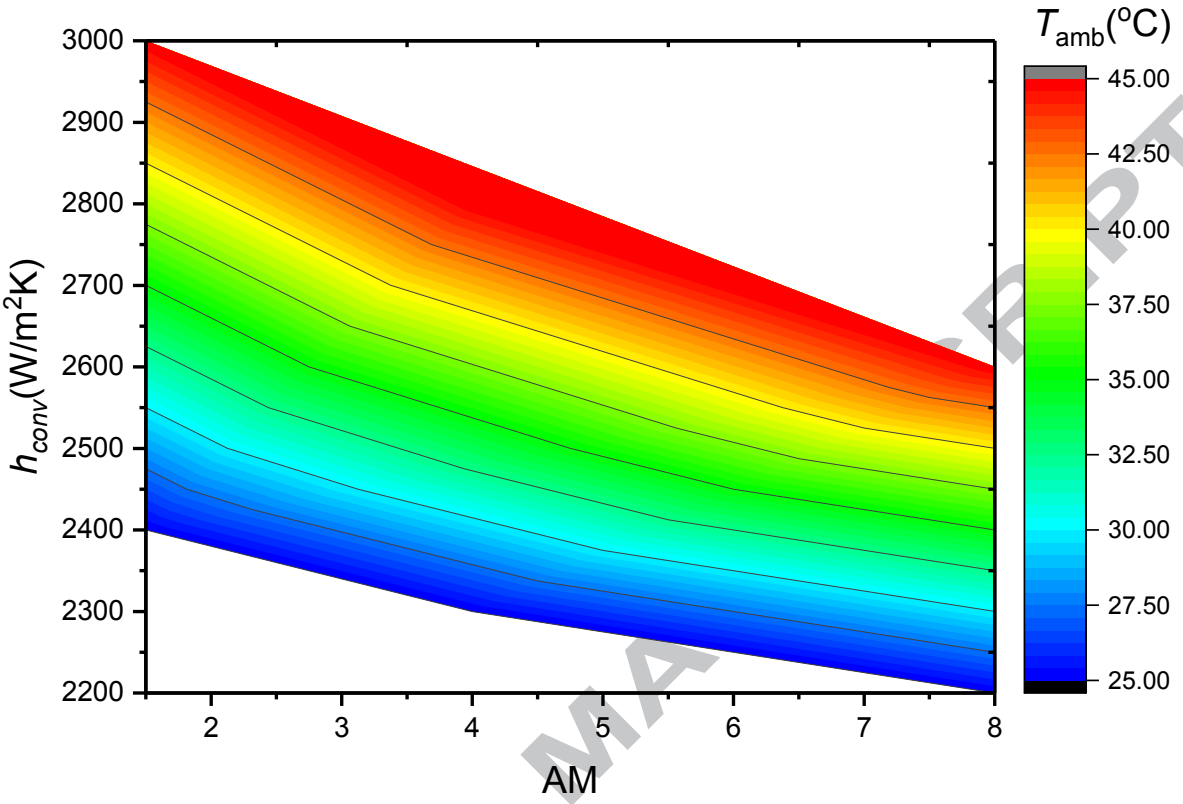


**Fig.15**. Variation values of $h_{conv}$ as a function of variation $T_{amb.}$ for the different of *AM*.

Figure 15 illustrates the significant impact of a higher ambient temperature, and lower value of air mass, on the solar cell's convergence temperature. Therefore, the thermal response through the values of the convection heat transfer coefficient needs to be increased at the back of the receiver in order to operate below 80 °C. In contrast, when the air mass values increase, the response values of the convection heat transfer coefficient decrease, and it's magnitude depends on environmental temperature.

The thermal resistance of $10^{-5}$ Km$^2$/W is needed for a concentration ratio of 1000x [20]. The design of the solar receiver for high concentrating photovoltaics must be below this thermal resistance of the materials at the back of the solar cells [5, 56].

## 5. Conclusions

In this study, the effect of the air mass atmospheric parameter on the performance of a triple-junction solar cell is presented. The values of *AM* from (*AM* =1-10D) was studied on a thermal-electrical model and the results are given in *J-V*, *PV* curves and overall cell efficiency. It has been shown that the weakness of the spectrum leads to a reduction in the performance parameters of series connected sub-cells of a multi-junction solar cell. The challenge in characterising multi-junction cells is the sensitivity to the incident spectrum, because of the effects of changes in the air mass.

The cell temperature is calculated by an iterative computational technique. The efficiency has been shown to drop remarkably to about 3.5% as air mass decreased from 1.5 to 8D at 1000x concentrating ratio. This lead to a reduction in the required $h_{\text{conv}}$ and heat power by the solar cells as summarised in Table-3.

Thermal behaviour was studied for a range of convective heat transfer values, ambient temperatures and air mass. The amount of heat transfer from the solar receiver ought to be maximised, in order to operate the cells more safely at the lowest possible temperature. Thus, as deduced at high ambient temperature there $h_{conv}$ needs to increase to retain cell temperature below 80 $^{o}$C. While as *AM* increases, the $h_{\text{conv}}$ values decrease because the heat power decreases. From the modelling results, we have a better understanding of the thermal behaviour of the receiver assembly.

## Highlights

- *J-V* Characterisation of the three component sub-cells of a triple-junction cell as a function of different *AM*.
- Prediction of cell temperature by an iteration technique that converges to find a steady operating temperature.
- Increases in air mass have a significant effect on thermal and electrical performance.

**Acknowledgement**

Many grateful thanks to the School of Engineering and Physical Sciences, Heriot-Watt University, United Kingdom, also many thanks to the Libyan Authority for Research Science and Technology.

## References

[1] Dimroth F, Kurtz S. High-efficiency multijunction solar cells. MRS bulletin. 2007;32(03):230-5.
[2] Ju X, Wang Z, Flamant G, Li P, Zhao W. Numerical analysis and optimization of a spectrum splitting concentration photovoltaic–thermoelectric hybrid system. Solar Energy. 2012;86(6):1941-54.
[3] Simon P. Phillips FDaAWB. high efficiency III-V Multi-junction solar cells". . Chapter IC-6 Solar Cells. 2012(Second Edition).
[4] Talavera D, Pérez-Higueras P, Ruíz-Arias J, Fernández E. Levelised cost of electricity in high concentrated photovoltaic grid connected systems: spatial analysis of Spain. Applied Energy. 2015;151:49-59.
[5] Rodrigo P, Micheli L, Almonacid F. The high-concentrator photovoltaic module. High Concentrator Photovoltaics: Springer; 2015. p. 115-51.
[6] Ruiz-Arias JA, Gueymard CA. Solar Resource for High-Concentrator Photovoltaic Applications. High Concentrator Photovoltaics: Springer; 2015. p. 261-302.
[7] Faine P, Kurtz SR, Riordan C, Olson J. The influence of spectral solar irradiance variations on the performance of selected single-junction and multijunction solar cells. Solar cells. 1991;31(3):259-78.
[8] Fernández EF, Almonacid F, Ruiz-Arias J, Soria-Moya A. Analysis of the spectral variations on the performance of high concentrator photovoltaic modules operating under different real climate conditions. Solar Energy Materials and Solar Cells. 2014;127:179-87.

[9] Araki K, Yamaguchi M. Influences of spectrum change to 3-junction concentrator cells. Solar energy materials and solar cells. 2003;75(3):707-14.
[10] Rabady RI. Optimized multi-junction photovoltaic solar cells for terrestrial applications. Solar Energy. 2014;106:72-81.
[11] Senthilarasu S, Fernández EF, Almonacid F, Mallick TK. Effects of spectral coupling on perovskite solar cells under diverse climatic conditions. Solar Energy Materials and Solar Cells. 2015;133:92-8.
[12] Broderick LZ, Albert BR, Pearson BS, Kimerling LC, Michel J. Design for energy: Modeling of spectrum, temperature and device structure dependences of solar cell energy production. Solar Energy Materials and Solar Cells. 2015;136:48-63.
[13] Ju X, Vossier A, Wang Z, Dollet A, Flamant G. An improved temperature estimation method for solar cells operating at high concentrations. Solar Energy. 2013;93(0):80- 9.
[14] Peharz G, Rodríguez JPF, Siefer G, Bett AW. A method for using CPV modules as temperature sensors and its application to rating procedures. Solar Energy Materials and Solar Cells. 2011;95(10):2734-44.
[15] Theristis M, Fernández EF, Stark C, O'Donovan TS. A theoretical analysis of the impact of atmospheric parameters on the spectral, electrical and thermal performance of a concentrating III–V triple-junction solar cell. Energy Conversion and Management. 2016;117:218-27.
[16] Almonacid F, Pérez-Higueras P, Fernández EF, Rodrigo P. Relation between the cell temperature of a HCPV module and atmospheric parameters. Solar Energy Materials and Solar Cells. 2012;105:322-7.
[17] Muñoz-Rodríguez FJ, Muñoz-Cerón E, Almonacid F, Fernández EF. Efficiencies and energy balance in high-concentrator photovoltaic devices. High Concentrator Photovoltaics: Springer; 2015. p. 239-60.
[18] Theristis M, O'Donovan TS. Electrical-thermal analysis of III–V triple-junction solar cells under variable spectra and ambient temperatures. Solar Energy. 2015;118:533-46.
[19] Theristis M, Stark C, O'Donovan TS. Determination of the cooling requirements for single cell photovoltaic receivers under variable atmospheric parameters. Conference Determination of the cooling requirements for single cell photovoltaic receivers under variable atmospheric parameters. IEEE, p. 1-5.
[20] Royne A, Dey CJ, Mills DR. Cooling of photovoltaic cells under concentrated illumination: a critical review. Solar energy materials and solar cells. 2005;86(4):451-83.
[21] Gualdi F, Arenas O, Vossier A, Dollet A, Aimez V, Arès R. Determining passive cooling limits in CPV using an analytical thermal model. Conference Determining passive cooling limits in CPV using an analytical thermal model, vol. 1556. AIP Publishing, p. 10-3.
[22] Aldossary A, Mahmoud S, Al-Dadah R. Technical feasibility study of passive and active cooling for concentrator PV in harsh environment. Applied Thermal Engineering. 2016;100:490-500.
[23] Espinet-González P, Algora C, Núñez N, Orlando V, Vázquez M, Bautista J, et al. Evaluation of the reliability of commercial concentrator triple-junction solar cells by means of accelerated life tests (ALT). Conference Evaluation of the reliability of commercial concentrator triple-junction solar cells by means of accelerated life tests (ALT), vol. 1556. AIP, p. 222-5.
[24] Gueymard C. Simple model of the atmospheric radiative transfer of sunshine (SMARTS2): algorithms and performance assessment. Florida: Solar Energy Center. 1995.
[25] Gueymard CA. Parameterized transmittance model for direct beam and circumsolar spectral irradiance. Solar Energy. 2001;71(5):325-46.
[26] Gueymard CA, Myers D. Solar resource for space and terrestrial applications. Solar Cells and Their Applications. 2010;217:427.
[27] Myers DR, Emery K, Gueymard C. Revising and validating spectral irradiance reference standards for photovoltaic performance evaluation. Journal of solar energy engineering. 2004;126(1):567-74.
[28] Peharz G, Siefer G, Bett A. A simple method for quantifying spectral impacts on multi-junction solar cells. Solar Energy. 2009;83(9):1588-98.

[29] Fernández EF, García-Loureiro AJ, Smestad GP. Multijunction concentrator solar cells: analysis and fundamentals. High Concentrator Photovoltaics: Springer; 2015. p. 9-37.
[30] Varshni YP. Temperature dependence of the energy gap in semiconductors. Physica. 1967;34(1):149-54.
[31] Multiphysics C. COMSOL multiphysics user guide (Version 4.3 a). COMSOL, AB. 2012:39-40.
[32] Micheli L, Fernández EF, Almonacid F, Mallick TK, Smestad GP. Performance, limits and economic perspectives for passive cooling of High Concentrator Photovoltaics. Solar Energy Materials and Solar Cells. 2016;153:164-78.
[33] Renno C, Petito F. Design and modeling of a concentrating photovoltaic thermal (CPV/T) system for a domestic application. Energy and Buildings. 2013;62:392-402.
[34] Sarhaddi F, Farahat S, Ajam H, Behzadmehr A, Adeli MM. An improved thermal and electrical model for a solar photovoltaic thermal (PV/T) air collector. Applied Energy. 2010;87(7):2328-39.
[35] Ceylan İ, Gürel AE, Ergün A, Tabak A. Performance analysis of a concentrated photovoltaic and thermal system. Solar Energy. 2016;129:217-23.
[36] Ota Y, Nagai H, Araki K, Nishioka K. Thermal transfer simulation for concentrator photovoltaic receiver under concentration condition. Conference Thermal transfer simulation for concentrator photovoltaic receiver under concentration condition, vol. 1556. AIP Publishing, p. 18-21.
[37] Fernández EF, Rodrigo P, Almonacid F, Pérez-Higueras P. A method for estimating cell temperature at the maximum power point of a HCPV module under actual operating conditions. Solar Energy Materials and Solar Cells. 2014;124:159-65.
[38] Jiji LM, Jiji LM. Heat convection: Springer, 2006.
[39] Verlinden P, Lasich J. Energy rating of concentrator PV systems using multi-junction III–V solar cells. Conference Energy rating of concentrator PV systems using multi-junction III–V solar cells. IEEE, p. 1-6.
[40] Kinsey GS, Edmondson KM. Spectral response and energy output of concentrator multijunction solar cells. Progress in Photovoltaics: Research and Applications. 2009;17(5):279-88.
[41] Helmers H, Schachtner M, Bett AW. Influence of temperature and irradiance on triple-junction solar subcells. Solar Energy Materials and Solar Cells. 2013;116:144-52.
[42] Fernández EF, Rodrigo P, Fernández J, Almonacid F, Pérez-Higueras P, García-Loureiro A, et al. Analysis of high concentrator photovoltaic modules in outdoor conditions: influence of direct normal irradiance, air temperature, and air mass. Journal of Renewable and Sustainable Energy. 2014;6(1):013102.
[43] Fernández EF, Pérez-Higueras P, Almonacid F, Loureiro AG, Fernández J, Rodrigo P, et al. Quantifying the effect of air temperature in CPV modules under outdoor conditions. Conference Quantifying the effect of air temperature in CPV modules under outdoor conditions, vol. 1477. AIP Publishing, p. 194-7.
[44] Meusel M, Adelhelm R, Dimroth F, Bett A, Warta W. Spectral mismatch correction and spectrometric characterization of monolithic III–V multi-junction solar cells. Progress in Photovoltaics: Research and Applications. 2002;10(4):243-55.
[45] García-Domingo B, Aguilera J, De la Casa J, Fuentes M. Modelling the influence of atmospheric conditions on the outdoor real performance of a CPV (Concentrated Photovoltaic) module. Energy. 2014;70:239-50.
[46] Sze SM, Ng KK. Physics of semiconductor devices: John wiley & sons, 2006.
[47] Philipps SP, Bett AW. III-V Multi-junction solar cells and concentrating photovoltaic (CPV) systems. Advanced Optical Technologies. 2014;3(5-6):469-78.
[48] Walker AW. Bandgap engineering of multi-junction solar cells using nanostructures for enhanced performance under concentrated illumination: University of Ottawa (Canada), 2013.
[49] Green M, Emery K, Hishikawa Y, Warta W, Dunlop E. Solar Cell Efficiency Tables (Version 38). Progress in Photovoltaics: Research and Applications. 2011;19(NREL/JA-5200-52449).

[50] Renno C, Petito F, Landi G, Neitzert H. Experimental characterization of a concentrating photovoltaic system varying the light concentration. Energy Conversion and Management. 2017;138:119-30.
[51] Muron A, Chowa S, Wheeldona J, Hinzera K, Schriemera H. Thermal optimization of a solar cell carrier for concentrator systems. Conference Thermal optimization of a solar cell carrier for concentrator systems, vol. 8007. p. 800722-1.
[52] Maka AO, O'Donovan TS. Modelling of the thermal behaviour of solar high concentrating photovoltaic receiver. Thermal Science and Engineering Progress. 2018.
[53] Frei W. Solutions to Linear Systems of Equations: Direct and Iterative Solvers. COMSOL Blog. 2013.
[54] Wang Z, Zhang H, Wen D, Zhao W, Zhou Z. Characterization of the InGaP/InGaAs/Ge triple-junction solar cell with a two-stage dish-style concentration system. Energy Conversion and Management. 2013;76:177-84.
[55] Peharz G, Ferrer Rodríguez JP, Siefer G, Bett AW. Investigations on the temperature dependence of CPV modules equipped with triple-junction solar cells. Progress in Photovoltaics: Research and Applications. 2011;19(1):54-60.
[56] Micheli L, Sarmah N, Luo X, Reddy K, Mallick TK. Opportunities and challenges in micro-and nano-technologies for concentrating photovoltaic cooling: A review. Renewable and Sustainable Energy Reviews. 2013;20:595-610.

# Conflict of Interest

No conflict of interest

## Highlights

- *J-V* Characterisation of the three component sub-cells of a triple-junction cell as a function of different *AM*.
- Prediction of cell temperature by an iteration technique that converges to find a stead operating temperature.
- Increases in air mass have a significant effect on the thermal and electrical performance.